

VMC: The Venus Monitoring Camera

W.J. Markiewicz¹, D.V. Titov^{1,4}, B. Fiethe², T. Behnke³, I. Szemerey¹, H. Perplies¹, M. Wedemeier¹, I. Sebastian¹, W. Boogaerts¹, C. Dierker², B. Osterloh², N. Ignatiev⁴, W. Böker¹, M. Koch², H.U. Keller¹, R. Jaumann³, H. Michaelis³, H. Michalik², D. Crisp⁵, L. Esposito⁶, S.S. Limaye⁷, S. Watanabe⁸, N. Thomas⁹, D. Belyaev⁴, A. Dannenberg¹, M. Tschimmel¹, R. Moissl¹, S.F. Hviid¹, T. Roatsch³ & K.-D. Matz³

¹*Max-Planck-Institute for Solar System Research, Max-Planck Str. 2, D-37191 Katlenburg-Lindau, Germany*

Email: markiewicz@mps.mpg.de

²*IDA, Technical University Braunschweig, Hans-Sommer-Str. 66, D-38106 Braunschweig, Germany*

³*German Aerospace Center (DLR), Rutherfordstrasse 2, D-12489 Berlin, Germany*

⁴*Space Research Institute (IKI), Profsoyuznaya Ulitsa 84/32, 117997 Moscow GSP-7, Russia*

⁵*Jet Propulsion Laboratory, 4800 Oak Grove Drive, Pasadena, CA 91109, USA*

⁶*Laboratory for Atmospheric and Space Physics, University of Colorado, Boulder, CO 80309-0392, USA*

⁷*Space Science and Engineering, University of Wisconsin, 1225 Dayton Street, Madison, WI 53706-1695, USA*

⁸*Hokkaido University, North 10, West 8, 060-0810 Sapporo, Japan*

⁹*Department of Space Research and Institute of Physics, University of Bern, Sidlerstr. 5, CH-3012 Bern, Switzerland*

Studying the dynamics of the Venus atmosphere, one of the main goals of the Venus Express mission, requires global imaging of the planet. The Venus Monitoring Camera (VMC) meets this goal by having the relatively wide field-of-view of 17.5°. VMC is recording images using four narrowband filters, from UV to near-IR, all sharing one CCD. The spatial resolution is 0.2–45 km per pixel, depending on the distance from the planet. The planet's full disc is captured near the apocentre of the orbit. VMC is complementing the mission's other instruments by tracking cloud motions at ~70 km (cloud tops) and at ~50 km (main cloud layer) altitudes, mapping oxygen night-glow and its variability, mapping the nightside thermal emission from the surface, and studying the lapse rate and water content in the lower 6–10 km. In addition, VMC is providing imaging context for the whole mission, and its movies of the atmosphere are of significant interest for science and the public outreach programme.

The Venus Express mission is focusing on the global investigation of the planet's atmosphere and plasma environment. It is also addressing important aspects of geology and surface physics. The core payload originally proposed for the mission consisted of instruments available from the Mars Express and Rosetta projects: SPICAM, PFS, ASPERA, VIRTIS and VeRa. This core payload, although capable of performing quality science at Venus, was missing a wide-angle imaging instrument. The only imager (VIRTIS) has a field-of-view of ~4°, far too narrow for routine observations of the global pattern of atmospheric motions. Complete coverage of the planet's disc by VIRTIS requires complex spacecraft repointing that is possible only at apocentre. The study of global dynamics is a major mission goal, so a relatively simple wide-angle camera was proposed with narrowband filters focusing on a few specific science goals. The

1. Introduction

paper describes VMC, its science goals, some of the key calibration data and operation modes at Venus. The original design foresaw six optical filters and two CCD detectors. Although it has partial heritage from Rosetta and Mars Express, VMC was a new development, and the limited time and resources forced a compromise to four channels and one CCD.

2. Scientific Objectives

The focus of VMC is to observe the atmosphere's dynamical phenomena from the thermosphere (~150 km) down to the main cloud deck (~50 km), as well as sounding the surface through the 1 μm transparency window.

2.1 Daytime observations in the UV–blue spectral range

The spectrum of solar radiation reflected by Venus has broad absorption feature between 0.2 μm and 0.5 μm (Moroz et al., 1985). The spectrum between 0.2 μm and 0.32 μm is well explained by the presence of SO_2 gas at the cloud tops. The spectrum above 0.32 μm implies the presence of another absorber that has not been identified so far; its identification is important because this species absorbs about 50% of the solar radiation. This has implications for the energy balance and dynamics of the whole atmosphere. Inhomogeneity in spatial and/or vertical distribution of the unknown absorber produces the famous UV features on the planet's disc (Fig. 1). Tracking their motions helps to study the dynamics of the cloud tops, measure wind speed and observe wave phenomena. The typical size of most of the UV features does not exceed 100 km. An exception is the global 'Y-feature'; its motion marks the super-rotation of the cloud tops at ~67 km altitude with zonal velocity of about 100 m/s and ten times slower meridional speed. With this objectives in mind, one of the VMC filters (UV) was chosen to cover the spectral range 350–385 nm, similar to that of the Pioneer Venus Orbiter cloud photopolarimeter (Colin & Hunten, 1977). It will be used to study:

- the spatial and vertical distribution of the UV–blue absorbers at the cloud tops;
- the dynamics of cloud tops by tracing the motions of UV features;
- the vertical distribution of haze above the main cloud layer.

2.2 Observations through the visible filter

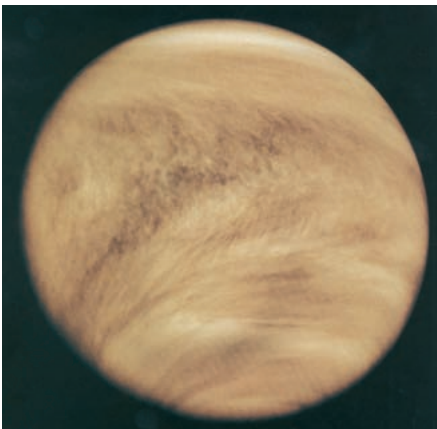
Several types of airglow have been observed on the Venus nightside (Crisp et al., 1996; Stewart et al., 1980). The Venera-9/10 spectrometer discovered a strong airglow in the visible (Krasnopolsky, 1983). The spectrum led to the unambiguous identification of the Herzberg I and II systems of O_2 with a total intensity of ~3 kR. Limb observations showed that this emission originates in a layer at 90–110 km altitude.

The second VMC filter (VIS) is positioned roughly in the middle of the Herzberg system, with the spectral range from 500 nm to 560 nm. Mapping the airglow spatial distribution and its temporal variations with this filter is contributing to the study of the circulation of the lower thermosphere (100–130 km). Limb imaging is being used to study the high-altitude haze layers. These observations are also continuing the search for lightning and measuring the visible albedo of Venus.

2.3 Surface and lower atmosphere emission in the 1 μm window

The discovery of spectral windows in the near-IR spectrum of Venus (Allen & Crawford, 1984), through which thermal radiation from the hot lower atmosphere and even surface can leak to space, provided a powerful tool to study the atmosphere below the clouds. These weak emissions can be observed only on the nightside. Fig. 2 shows a synthetic spectrum of the nightside (Ignatiev, private communication). It compares well with that measured by the VIMS

Fig. 1. Mariner-10 image of Venus, showing the UV markings.



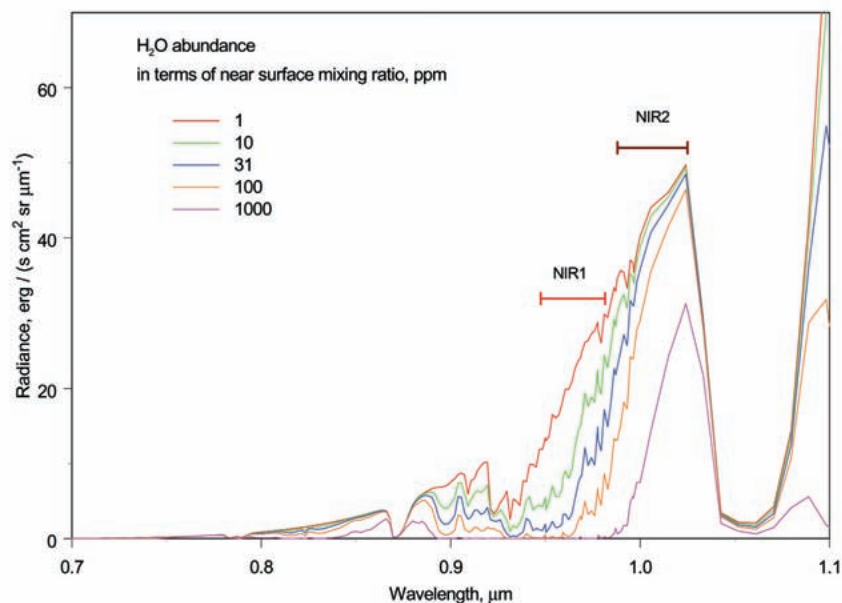


Fig. 2. Synthetic spectrum of the radiation from the Venus nightside.

Fig. 3 Ground-based observations of the nightside in the 1 μm transparency window.



instrument during the Cassini flyby (Baines et al., 2000). Ground-based observations (Fig. 3) and subsequent radiative transfer modelling show that the 1 μm window emission originates at the surface (Meadows & Crisp, 1996). The thick atmosphere and cloud layer contribute only to conservative scattering of the radiation but not to emission.

2.4 Dayside observations in the near-IR filters

Observations via two near-IR filters on the dayside are being used to map the water vapour abundance at the cloud tops. The measurements with the NIR2 filter is also being used to study variations of the total cloud optical depth and atmospheric motions in the main cloud deck, although the brightness contrasts are very low ($\sim 1\%$).

3.1 Overview and accommodation

The 1.50 kg VMC consists of a single unit that houses the optics, CCD and readout electronics (CRE), digital processing unit (DPU), and the power converter (POC) (Fig. 4). A Peltier element connected to the bottom of the CCD cools the detector. In order to avoid moving parts such as a filter wheel, the camera is designed so that the four objectives (channels) share a single CCD. Straylight protection is provided by external and internal baffles. The camera is mounted on the +Y wall inside the spacecraft. A performance summary of VMC is given in Table 1.

The image data from the CCD are read out by the CRE and sent to the 1 Gbit mass memory integrated within the DPU. This DPU uses the miniaturised ‘system-on a chip’ approach, which integrates all DPU functions into a single chip. The processor is based on a LEON-2 SPARC V8-compatible core, implemented in a radiation-hardened Xilinx Virtex field-programmable gate array. Before image data are sent to the spacecraft via the high-speed IEEE 1355 interface, different image-processing functions (e.g. flat-fielding or JPEG2000 compression) can be done in realtime or offline. All VMC internal functions can be configured by the built-in ‘On-board Command Language’ (OCL), which allows the execution of user-definable scripts in parallel working virtual machines.

3. The Instrument



Fig. 4. VMC with one side of the housing removed, showing the CRE, DPU and POC boards (top to bottom).

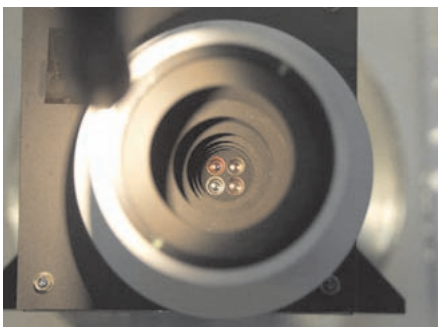


Fig. 5. The front (top) and rear of the VMC optics.

Table 1. The principal characteristics of VMC.	
Item	Specification
<i>Optics</i>	
General concept	Four objectives sharing a single CCD
Total field of view	~17.5° (0.3 rad)
Image scale	~0.74 mrad/px
<i>Detector and CCD readout electronics (CRE)</i>	
Type	Kodak KAI-1010, front illuminated, interline architecture, antiblooming
Detector size	1032(H)x1024(V)
Pixel size	9.0x9.0 mm
Full well	30 000 electrons
Total noise	~100 e @ +37°C
Dark current	~3000 x 2 ^[-(40-T_c)/8] e/s/px
Readout frequency	2.08896 MHz
Integration time	N x 0.504 ms, N = 1, 2, 3...64449
Power consumption	2.0 W secondary
Operational temperature range	-30°C to +50°C
Non-op. temperature range	-50°C to 70°C
<i>Digital Processing Unit (DPU)</i>	
Processor	LEON-2 core (SPARC-compatible) 20 MIPS
Memory	1 Gbit image mass storage (SDRAM) 16 Mbit SRAM 16 Mbit EEPROM (program memory) 64 kbit PROM (Bootloader)
Power consumption	3.2 W secondary
<i>Power Converter (POC)</i>	
Converter	4 Delta/VPT RT Converter
Power consumption	Efficiency = 0.5...0.75

Table 3. VMC mode characteristics.			
	<i>Pericentre</i>	<i>Monitoring</i>	<i>Limb</i>
Distance (km)	250–10 000	10 000–66 000	~2000
Total field-of-view (km)	70–3000	3000–20 000	~500
Spatial resolution (km)	0.2–7	7–45	~1.5
Time between images	5–300 s	~10 min	~ 10 s

3.2 Optical design

Four independent optical channels share one CCD; the optical design is presented in Table 2. The optics (Fig. 5) were manufactured by FISBA OPTIK of St. Gallen (CH).

‘Ghost images’ inside a CCD camera result from multiple reflections between the CCD surface and the surfaces of the lens. The reflected light returns to the CCD and produces a secondary image in a different position on the CCD than the primary. Although this secondary image is normally much weaker than the primary, it is of crucial importance in observing the nightside of Venus: the nightside emission is so weak that it is completely dominated by the ghost of the dayside crescent. To suppress the ghost image, an absorbing light-trapping disc

Table 2. The VMC optical characteristics.

VMC Channel	VIS	NIR1	NIR2	UV
Spectral range	500–560 nm	950–990 nm	990–1030 nm	350–385 nm
Centre wavelength	513 nm	965 nm	1.0 μm	365 nm
Focal length	13 mm	13 mm	13 mm	13 mm
F-number	5	5	5	7
Optics	3 identical Cooke Triplets + curved front filter			separate Cooke Triplet + curved front filter
Stop/obscuration	central	central	central	none
CCD	Kodak KAI-1010 Series, 1024x1024 pixel interline CCD, 9 μm pixel pitch			
Used area for imaging	#1 CCD quadrant	#2 CCD quadrant	#3 CCD quadrant	#4 CCD quadrant
Optical layout				

was glued in the stops of the VIS and both NIR optics. This obscuration spot can be seen in the VIS channel showing the green ring in Fig. 5. Ghosts are completely suppressed and could not be seen in the VMC calibration images.

VMC has several operation modes to cover all possible observation goals and conditions; Table 3 summarises their principal characteristics. The modes are pericentre, transmission, monitoring and limb:

- the pericentre mode is used to study small-scale dynamics and the fine cloud structure at high resolution. It is used when the spacecraft is within 250–10 000 km of the planet, where it is the only imaging instrument. The images collected during a pericentre pass are stored in the VMC internal memory and sent to the spacecraft afterwards in transmission mode.
- the monitoring mode is used to study global atmospheric dynamics from a distance for relatively long periods: ~ 8 h in the ascending arc of the orbit or ~ 2 h around pericentre.
- in the limb mode, VMC is used to study the vertical structure of atmospheric hazes above the clouds.

This section briefly describes the VMC properties and behaviour that were investigated during the on-ground instrument characterisation. The analysis of the radiometric calibration data was still not completed at the time of writing. Figure 6 shows an example of a VMC flat field taken during the calibration campaign.

5.1 CCD performance

To verify the electro-optical performance of the detector, including the readout electronics, the photon-transfer technique was used to specify total noise in darkness and system gain. Images were acquired with and without light using different exposure times; the measured linearity error of the CCD is less than 1%. Fig. 7 shows the measured quantum efficiency of the the CCD together with approximate positions of the filters (indicated by the horizontal bars). To separate the noise performance of the detector from that of the readout electronics, the CRE electronics were thermal-vacuum tested without the CCD.

4. Science Operations

5. Calibration and Performance

Fig. 6 (left). The VMC flat field, showing the four channels on one CCD.

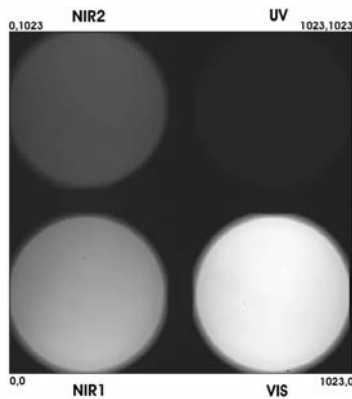


Fig. 7 (right). The CCD's measured quantum efficiency (QE).

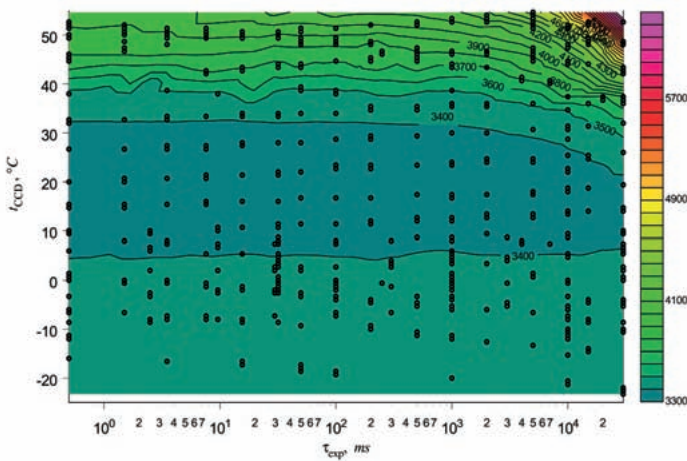
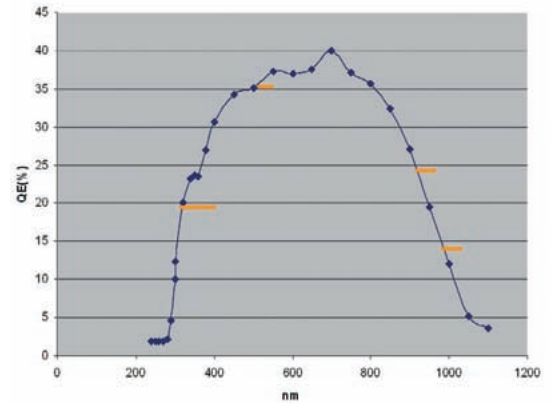


Fig. 8. Dark signal as a function of the exposure time and CCD temperature, averaged over the whole matrix except hot pixels and shaded boundary frame. The measurement points are shown as black circles.

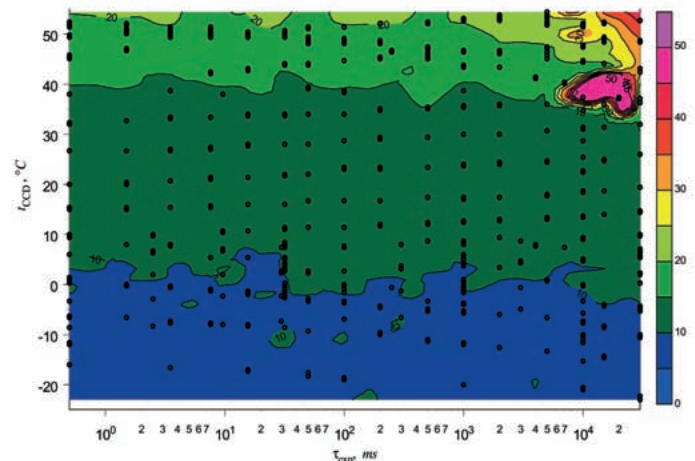


Fig. 9. Dark signal noise as a function of the exposure time and CCD temperature, averaged over the whole matrix except hot pixels and shaded boundary frame. The measurement points are shown as black circles.

In this configuration, the CRE electronics input was grounded (no CCD). The noise of the readout electronics is of the order of five electrons at 2 MHz pixel frequency. As expected, the exposure time control had no influence.

5.2 Focus measurements

The focus measurements on the VIS channel on-axis were performed several times between environmental tests in order to confirm that vibration and thermal-vacuum tests had not distorted the focus. A full focus test for all four channels was performed under laboratory calibration at three temperatures: room, 40°C, and -20°C. In all cases, defocusing was not detected or was low and within the range of depth-of-field of ±25 μm. The hot case, with a camera temperature of 36°C and CCD temperature of 48°C, resulted in a just-acceptable camera defocus of +30 μm.

5.3 Dark signal properties

5.3.1 Dark signal behaviour with temperature and exposure

The VMC dark signal is the sum of the dark current (a function of temperature and exposure time) and the bias, a constant electronics offset of about 3300–3400 DN. Fig. 8 shows the dependence of the dark signal with temperature and exposure time. For temperatures below ~35°C and all available

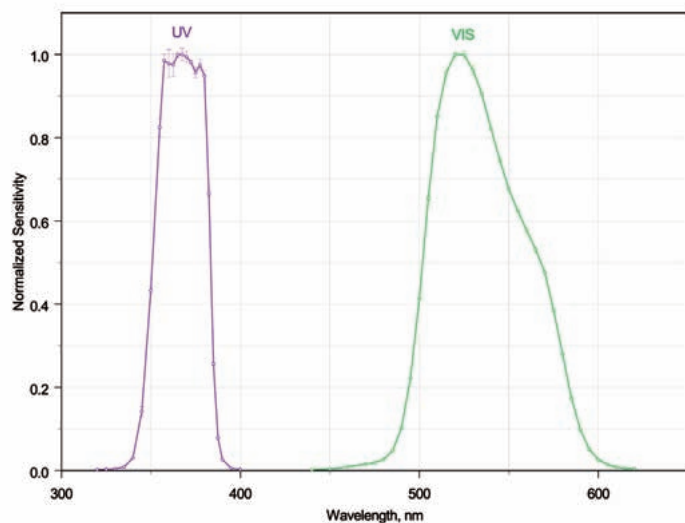


Fig. 10. Normalised spectral sensitivities of the UV and VIS channels.

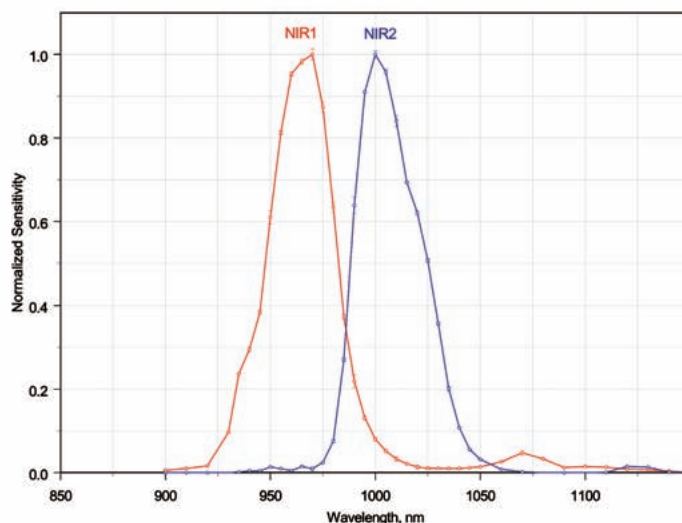


Fig. 11. Normalised spectral sensitivities of the NIR channels.

exposures (0.5 ms to 30 s), the dark signal is defined by the bias. At temperatures above 40°C the increase of dark current with temperature becomes dominant.

5.3.2 Dark signal noise

Figure 9 shows the field of dark signal noise as a function of exposure time and the CCD temperature. This plot represents the standard deviation of the CCD counts obtained by subtraction of two images taken one after another using the same exposure time. Except for the region of high temperatures and long exposures, the dark noise is below 25 DNs, which is close to the standalone CCD noise. Note that the standard deviation of the dark signal in each single image is much higher, which indicates that each CCD pixel behaves individually and that a matrix of dark current noise instead of a single value should be used for dark current correction.

5.4 Spectral properties

The spectral properties of the four channels were determined by laboratory calibration; they are shown in Fig. 10 and Fig. 11.

5.5 Expected flight performance

Simulation of flight operations during the VMC thermal-vacuum tests together with numerical modelling of the spacecraft's thermal behaviour in typical orbital cases carried out by Astrium, allows the CCD's flight temperatures to be predicted. An important conclusion is that, for all planned observations, the CCD temperature falls in the optimal domain in which dark signal and dark noise are close to their minimal values and have weak dependence on CCD temperature and exposure time.

Allen, D. & Crawford, J.W. (1984). Cloud Structure on the Dark Side of Venus. *Nature* **307**, 222–224.

Baines, K., Bellucci, G., Bibring, J.-P., Brown, R.H., Buratti, B.J., Bussoletti, E., Capaccioni, F., Cerroni, P., Clark, R.N., Coradini, A., Cruikshank, D.P., Drossart, P., Formisano, V., Jaumann, R., Langevin, Y., Matson, D.L.,

References

- McCord, T.B., Mennella, T.B., Nelson, R.M., Nicholson, P.D., Sicardi, B., Sotin, C., Hansen, G.B., Aiello, J.J. & Amici, S. (2000). Detection of Sub-micron Radiation from the Surface of Venus by Cassini/VIMS. *Icarus* **148**, 307–311.
- Colin, L. & Hunten, D.M. (1977). Pioneer Venus Experiment Descriptions. *Space Sci. Rev.* **20**, 451–525.
- Crisp, D., Meadows, V.S., Bezdard, B., de Bergh, C., Maillard, J.-P. & Mills, F.P. (1996). Ground-based Near-infrared Observations of the Venus Nightside: 1.27 μm O_2 ($\alpha^1\Delta_g$) Airglow from the Upper Atmosphere. *J. Geophys. Res.* **101**, E2, 4577–4593.
- Krasnopolsky, V.A. (1983). Venus Spectroscopy in the 3000–8000 $^\circ\text{C}$ Region by Veneras 9 and 10. In *Venus-I* (Eds. D.M. Hunten, L. Colin, T.M. Donahue & V.I. Moroz), The University of Arizona Press, Arizona, USA, pp459-483.
- Meadows, V.S. & Crisp, D. (1996). Ground-based Near-infrared Observations of the Venus Nightside: The Thermal Structure and Water Abundance near the Surface. *J. Geophys. Res.* **101**, E2, 4595–4622.
- Moroz, V.I., Ekonomov, A.P., Moshkin, B.E., Revercomb, H.E., Sromovsky, L.A., Schofield, J.T., Spankuch, D., Taylor, F.W. & Tomasko, M.G. (1985). Solar and Thermal Radiation in the Venus Atmosphere. *Adv. Space Res.* **5**, 11, 197–232.
- Stewart, A.I.F., Gerard, J.-C., Rusch, D.W. & Bougher, S.W. (1980). Morphology of the Venus Ultraviolet Night Airglow. *J. Geophys. Res.* **85**, A13, 77861–7870.